Journal of Electroanalytical Chemistry 717-718 (2014) 96–102

Contents lists available at ScienceDirect

Journal of Electroanalytical Chemistry

journal homepage: www.elsevier.com/locate/jelechem

Graphene–polyamidoamine dendrimer–Pt nanoparticles hybrid nanomaterial for the preparation of mediatorless enzyme biosensor

Elena Araque, Christian B. Arenas, María Gamella, Julio Reviejo, Reynaldo Villalonga *, José M. Pingarrón *

Department of Analytical Chemistry, Faculty of Chemistry, Complutense University of Madrid, 28040 Madrid, Spain

ARTICLE INFO

Article history:
Received 8 October 2013
Received in revised form 27 November 2013
Accepted 10 January 2014
Available online 21 January 2014

Keywords:
Dendrimer
Enzyme biosensor
Glucose oxidase
Graphene
Platinum nanoparticles

ABSTRACT

A novel inorganic–organic hybrid nanomaterial was prepared by anchoring (3-glycidyloxypropyl)trimethoxysilane at the surface of graphene oxide, further cross-linking with polyamidoamine G-4 dendrimer, and final decoration with platinum nanoparticles. A glassy carbon electrode was coated with this hybrid nanomaterial and then used as support for the covalent immobilization of glucose oxidase. This enzyme electrode was employed to construct a mediatorless glucose amperometric biosensor. The resulting biosensor exhibited good electrocatalytical activity for the oxidation of the H_2O_2 produced by the enzyme catalyzed reaction, being able to detect glucose when poised at +400 mV. The biosensor showed a wide linear response to glucose ranging from 10 μM to 8.1 mM, high sensitivity of 24.6 mA/M cm^2 and low detection limit of 0.8 μM. The biosensor was successfully tested for the quantification of glucose in samples of commercial soft drinks.

1. Introduction

During the last years, the use of functional nanomaterials to design electrochemical biosensors with improved stability and analytical performance has been largely explored [1–3]. Nanosized materials have been employed to tailor the chemical and physical properties of electrode surfaces allowing an efficient immobilization of biologically active biomolecules and occurrence of the electrochemical processes involved in the electroanalytical application. In addition, nanomaterials have proven to be useful tools for achieving amplification and providing biorecognition-signaling elements to prepare novel generation electrochemical biosensors [4,5].

In this context, special interest has attracted the design of novel hybrid nanomaterials for electroanalytical applications [6,7]. This unique type of nanomaterials not only offers the advantages associated to combine components of different nature (i.e. organic and inorganic adducts) into the same material, but also provides the possibility to tailor-made the physical and chemical properties of the resulting hybrid through the rational combination of selected functional components [8].

Graphene constitute an excellent candidate for the preparation of nanosized hybrid materials for biosensing due to its unique properties such as large surface-to-volume ratio, easy and cost-effective synthesis and exceptional high electrical conductivity, mechanical strength and thermal stability [9,10]. In addition, new or improved characteristics such as solubility, chemical functionality, wettability and catalytic capacity can be conferred to graphene by appropriate chemical or physical hybridization with other materials.

A variety of electrochemical biosensors has been constructed by using organic–organic and organic–inorganic hybrid nanomaterials involving the combination of graphene with metal nanoparticles, natural and synthetic polymers and metal/non-metal oxide nanostructures. Gold nanoparticles adsorbed on polyvinylpyrrolidone-protected graphene were included into a chitosan film and this hybrid nanomaterial was used as support for the immobilization of glucose oxidase (GOx) and the amperometric detection of glucose [11]. Similarly, Wu et al. reported the electrodeposition of Pt nanoparticles on glassy carbon electrodes coated with graphene/chitosan, and the further immobilization of GOx for glucose biosensing [12].

Luo et al. recently described the non-covalent coating of graphene oxide with carboxyl-terminated PAMAM dendrimer, generation 3.5, and its further decoration with silver nanoparticles [13]. This hybrid nanomaterial was employed to construct an enzyme biosensor for glucose. Moreover, acetylcholinesterase was immobilized on glassy carbon electrodes coated with 3-carboxyphenylboronic/reduced graphene oxide/chitosan/gold nanoparticles hybrid nanocomposite, and used to detect organophosphorus and carbamate pesticides [14]. Guo et al. reported the construction of an electrochemical label-free integrated aptasensor using silver microspheres as a separation element and graphene-mesoporous silica-gold nanoparticle hybrids as an enhanced element of the sensing

* Corresponding authors. Tel.: +34 91 3944315; fax: +34 91 3944329 (J.M. Pingarrón).
E-mail addresses: rvillalonga@quim.ucm.es (R. Villalonga), pingarro@quim.ucm.es (J.M. Pingarrón).

1572-6657/$ - see front matter © 2014 Elsevier B.V. All rights reserved.
http://dx.doi.org/10.1016/j.jelechem.2014.01.016

platform for the detection of adenosine-5′-triphosphate as model compound [15].

Recently we reported the preparation of crumpled graphene-based nanoparticles by an initial modification of graphene oxide with (3-glycidyloxypropyl)trimethoxysilane and further cross-linking with four-generation ethylenediamine core polyamidoamine dendrimer (PAMAM) [16]. This organic–organic hybrid nanomaterial (PAMAM-Sil-rGO) was employed to construct a tyrosinase biosensor for the quantification of cathecol. In this work we describe the use of this graphene derivative to prepare a novel organic–inorganic hybrid nanomaterial by decoration of PAMAM-Sil-rGO derivative with Pt nanoparticles (PtNPs/PAMAM-Sil-rGO). This hybrid nanomaterial was tested as an appropriate scaffold to design a mediatorless amperometric biosensor for glucose.

2. Materials and methods

2.1. Materials

Graphene oxide, prepared according to Hummers method [17], was acquired from NanoInnova Technologies (Spain). Glucose oxidase (GOx, 174 kU/mg), (3-glycidyloxypropyl)trimethoxysilane (GPTMS), glucose colorimetric assay kit, $H_2PtCl_6{\cdot}6H_2O$, $NaBH_4$ and glutaraldehyde were purchased from Sigma–Aldrich Co. (USA). PAMAM was purchased from Dendritech, Inc. (USA). All other chemicals were analytical grade.

2.2. Electrochemical measurements

Electrochemical experiments were carried out with a three-electrode system, consisting of a glassy carbon electrode (GCE, 3.0 mm diameter) coated with GOx-modified graphene-based hybrid nanomaterial as working electrode, an Ag/AgCl/KCl (3 M) as reference electrode and a Pt wire as counter electrode. Electrochemical impedance spectroscopy and cyclic voltammetry were performed with a FRA2 μAutolab Type III potentiostat/galvanostat (Metrohm Autolab B.V., The Netherlands). Amperometric measurements were carried out with a dual-channel Inbea potentiostat (Inbea Biosensores S.L., Spain). Electrochemical impedance spectroscopy experiments were carried out in 0.1 M KCl solution containing 5 mM $K_3[Fe(CN)_6]/K_4[Fe(CN)_6]$ (1:1). Cyclic voltammetry and amperometric measurements were carried out in 0.1 M sodium phosphate buffer, pH 7.5 (working volume 10 mL). Freshly prepared solutions of 100 μM glucose in 50 mM sodium phosphate buffer, pH 7.5, were employed for biosensing experiments.

2.3. Microscopy analysis

Transmission electron microscopy (TEM) measurements were performed with a JEOL JEM-2000 FX microscope (JEOL Ltd., Japan). The morphology of the nanostructured electrode surfaces was studied by high resolution field emission scanning electron microscopy (FE-SEM) using a JEOL JSM-6335F apparatus (JEOL Ltd., Japan).

2.4. Preparation of the enzyme electrode (GOx/PtNPs/PAMAM-Sil-rGO/GCE)

PAMAM-Sil-rGO was prepared as previously described [16]. Briefly, 50 mg of graphene oxide was dispersed in 250 mL ethanol by sonication for 1 h. The resulting dispersion was then heated at 65 °C, mixed with 25 mL of a 1% (v/v) ethanolic solution of (3-glycidyloxypropyl)trimethoxysilane and kept under continuous stirring at this temperature during 12 h. The mixture was cooled, filtered, and the resulting solid containing the silanized graphene derivative was exhaustively washed with ethanol and finally dried in vacuum.

To prepare PAMAM-Sil-rGO, 50 mg of silanized graphene were dispersed in 200 mL ethanol by sonication and further mixed with 2.5 mL of 10% (w/w) ethylenediamine core PAMAM G-4 solution in methanol. The mixture was stirred at room temperature for 12 h, then filtered and the solid washed several times with ethanol. The dendrimer-modified graphene derivative was dried under vacuum at room temperature and kept in dessicator until use.

To prepare the enzyme electrode, a GCE was polished to a mirror-like finish using 0.3 μm alumina slurry and sonicated in distilled water and ethanol. The electrode was first coated with PAMAM-Sil-rGO by depositing two 10-μL aliquots of a 0.5 mg/mL aqueous dispersion of the nanomaterial on the electrode surface and allowing drying. The modified electrode was then dipped into a 10 mM sodium phosphate buffer solution, pH 5.0, and the potential was cycled between 0.0 and −1.5 V for 20 cycles to obtain a reduced graphene derivative on the electrode surface [18]. 20 μL of 5 mM H_2PtCl_6 (40 μg) aqueous solution were further dropped on the dried electrode and kept during 30 min at room temperature. Thereafter, 10 μL of 1 mM $NaBH_4$ solution were added and the reaction was allowed proceeding for 30 min. The modified electrode was exhaustively washed with distilled water to remove the non-adsorbed nanoparticles. GOx was further immobilized on the nanostructured electrode by dropping 16 μL of 7.5 mg/mL enzyme solution in 100 mM sodium phosphate buffer, pH 7.5, and mixing with 4 μL of 25% (v/v) glutaraldehyde. The electrode was kept at 4 °C for 1 h, then washed several times with cold 100 mM sodium phosphate buffer, pH 7.5 and finally stored in refrigerator until use.

3. Results and discussion

Fig. 1 illustrates the experimental protocol employed to prepare the organic–inorganic PtNPs/PAMAM-Sil-rGO hybrid nanomaterial on the electrode surface, and its further use as support for the covalent immobilization of GOx for biosensing purposes. PAMAM-Sil-rGO was prepared as previously described by Araque et al. [16] and it was used as coating material for the GCE. This nanomaterial was further decorated with Pt nanoparticles by incubation with H_2PtCl_6 aqueous solution and subsequent treatment with $NaBH_4$. TEM analysis revealed the formation of small and non-spherical Pt nanoparticles with average size of 3.3 ± 0.7 nm on the graphene sheets (Fig. 2A). These nanoparticles were mainly arranged in bunches-like structures on the nanocarbon sheets, as it was also observed by FE-SEM (Fig. 2C). The formation of such three-dimensional arrangements can be attributed to the inclusion of the nanoparticles into the interstitial volume of the hyperbranched PAMAM moieties, as a consequence of the stabilization of the growing colloids by the different amine groups of the dendrimer. Similar inclusion/stabilization was described for noble metal nanoparticles growth in the presence of PAMAM dendrimers of different generations [19,20].

It should be noted that the PtNPs/PAMAM-Sil-rGO nanosheets exhibited a less crumpled shape that the initial organic–organic hybrid nanomaterial [16], suggesting that the inclusion of the Pt nanoparticles into the dendrimer moieties caused an expansion of the nanomaterial. This change in the morphology of the graphene-based material could be also associated to the reduction process with $NaBH_4$.

Cyclic voltammetric studies revealed that this organic–inorganic hybrid nanomaterial showed high electrocatalytic activity toward decomposition of H_2O_2 (Fig. 3), as expected by the non-spherical shape of the Pt nanoparticles and their high load on the graphene nanomaterial. Thus, PtNPs/PAMAM-Sil-rGO was evaluated for the construction of a mediatorless oxidase-based electrochemical

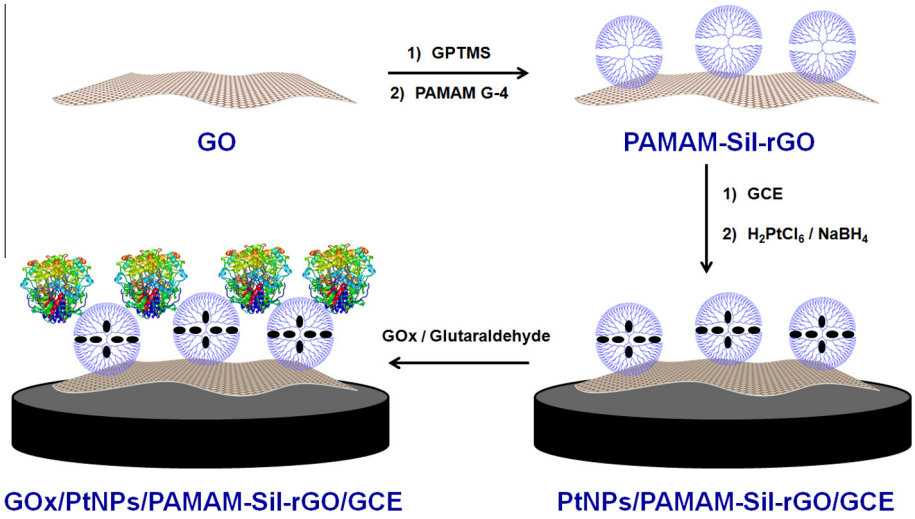

Fig. 1. Schematic display of the preparation of the GOx/PtNPs/PAMAM-Sil-rGO/GCE enzyme electrode.

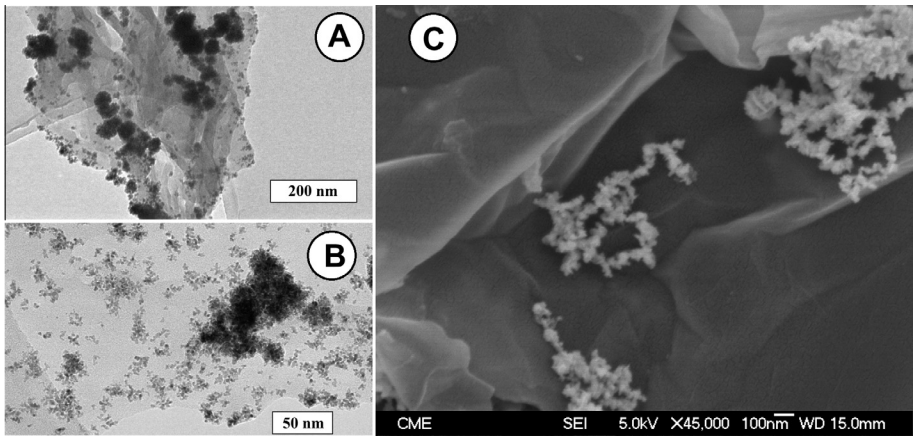

Fig. 2. TEM (A, B) and FE-SEM (C) images of PtNPs/PAMAM-Sil-rGO hybrid nanomaterial.

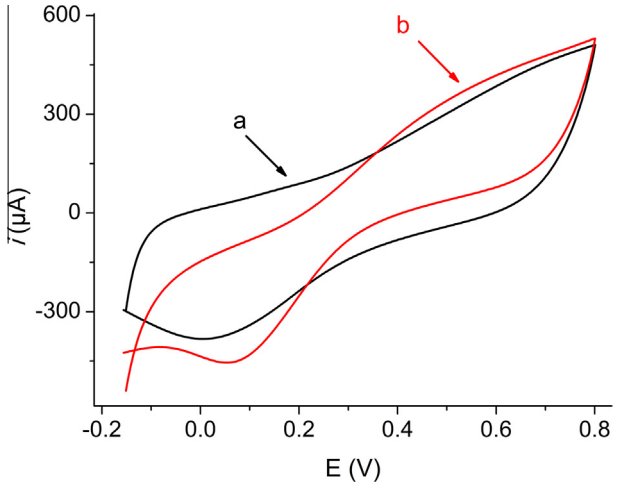

Fig. 3. Cyclic voltammograms of PtNPs/PAMAM-Sil-rGO/GCE in the absence (a) and in the presence (b) of 1 mM H_2O_2. Scan rate, 50 mV/s in 0.1 M sodium phosphate buffer, pH 7.0.

biosensor using GOx as model enzyme. GOx was immobilized on the nanostructured electrode by covalent attachment to the primary amino groups at the surface of PAMAM dendrimers using glutaraldehyde as cross-linking agent.

The preparation of the enzyme electrode was optimized by determining the influence of the experimental variables affecting the amperometric response of the nanostructured electrode towards glucose. Fig. 4A shows the effect of the PAMAM-Sil-rGO loading on the response of the GOx-based electrode upon addition of glucose using +400 mV as detection potential. The relative amperometric response with respect to the highest one increased with the hybrid nanomaterial loading up to 12.5 μg, which could be ascribed to the increased amount of free amino groups on the electrode surface accessible for enzyme immobilization. Larger hybrid nanomaterial loadings resulted in lower amperometric response, probably due to the formation of multilayer structures on the electrode surface then causing steric hindrance for enzyme immobilization and thus reducing the amount of active GOx on the biosensing interface. Accordingly, 12.5 μg of PAMAM-Sil-rGO were employed to coat the GCE in further experiments.

On the other hand, the electrochemical response of the biosensor increased progressively with the amount of GOx loaded on the nanostructured electrode surface, reaching the highest value when 150 μg of enzyme were immobilized on the PAMAM-Sil-rGO modified CGE (Fig. 4B). This behavior could be justified by the progressive attachment of a catalytically active enzyme layer attached on the PAMAM moieties. Lower electroanalytical response

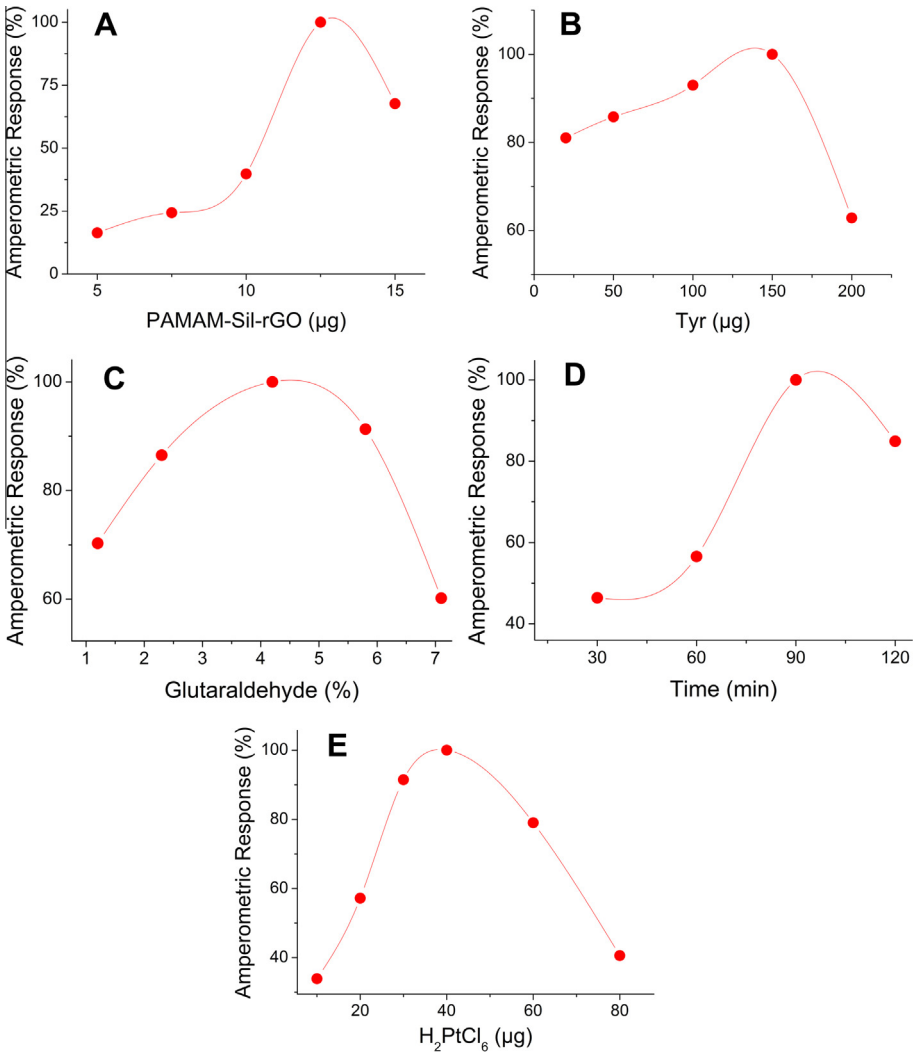

Fig. 4. Influence of the PAMAM-Sil-rGO loading (A), enzyme loading (B), glutaraldehyde concentration (C), incubation time (D) and amount of H_2PtCl_6 (E) on the normalized amperometric response of the GOx/PtNPs/PAMAM-Sil-rGO/GCE enzyme electrode toward 1 mM glucose. E = +400 mV.

was observed when higher amount of enzyme was loaded on the electrode surface which could be ascribed to the assembly of a second protein layer on the electrode surface that may form enzyme–enzyme cross-linked adducts with lower catalytic activity due to steric hindrance effects.

The effect of glutaraldehyde concentration on the amperometric response of the enzyme electrode is shown in Fig. 4C. A bell-shaped curve was observed with the highest current being provided at 4% glutaraldehyde. It could be expected that an increased amount of glutaraldehyde allowed higher amount of enzyme molecules to be attached to the electrode surface through stable covalent cross-linking. However, a relative high amount of glutaraldehyde could provoke intra- and intermolecular cross-linking of enzyme molecules yielding more rigid protein conformations with lower catalytic activity. In addition, high concentration of glutaraldehyde could provoke inactivation of GOx by modification of amino acid residues at the active site of the enzyme.

The influence of the immobilization time on the biosensor response is shown in Fig. 4D. Maximum electroanalytical signal was observed when the cross-linking process was performed during 90 min at 4 °C. Higher reaction times led to lower analytical response probably due to the partial inactivation of the attached enzyme molecules under exhaustive treatment with the cross-linking agent as commented above. At this point, it should be remarked that the decoration of PAMAM-Sil-rGO with Pt nanoparticles was carried out by using 40 μg of H_2PtCl_6 to ensure maximum amperometric response of the biosensor, according to the results shown in Fig. 4E. It could be expected that Pt nanoparticles are stabilized into the PAMAM-Sil-rGO hybrid nanomaterial by electrostatic interaction with the different amine groups of the dendrimer [19,20]. Accordingly, a large amount of primary amino groups could be involved in such nanoparticles stabilization when large amount of H_2PtCl_6 is reduced on the electrode surface, then lowering their availability to attach enzyme molecules during the immobilization process.

The assembly of the GOx/PtNPs/PAMAM-Sil-rGO/GCE electrode under the optimum conditions described above was tested by cyclic voltammetry and electrochemical impedance spectroscopy (EIS). Fig. 5 shows the cyclic voltammograms recorded at different stages of the modified enzyme electrode preparation in a 0.1 M KCl solution containing 5 mM $[Fe(CN)_6]^{4-/3-}$ ions. All electrode architectures showed well-defined quasi-reversible voltamperometric patterns, suggesting high electroconductive properties for the different surfaces which allow the fast diffusion of the electrochemical probe to the electrode. Actually, the GCE, PAMAM-Sil-rGO, PtNPs/PAMAM-Sil-rGO/GCE and GOx/PtNPs/PAMAM-Sil-rGO/GCE showed values for ΔE = 181 mV, 169 mV, 171 mV and 236 mV and i_a/i_c = 1.09, 1.06, 0.99 and 1.02, respectively.

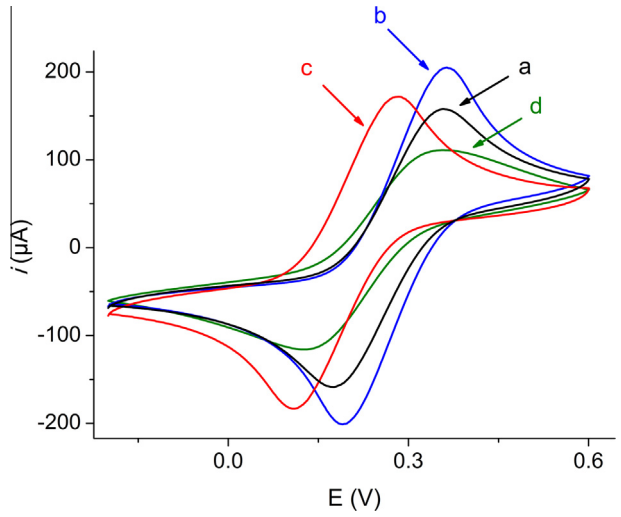

Fig. 5. Cyclic voltammograms on the bare GCE (a), PAMAM-Sil-rGO (b), PtNPs/PAMAM-Sil-rGO/GCE (c) and GOx/PtNPs/PAMAM-Sil-rGO/GCE (d) electrodes in 0.1 M KCl solution containing 5 mM $K_3[Fe(CN)_6]/K_4[Fe(CN)_6]$ (1:1). Scan rate: 50 mV/s.

The electrochemical surface area of the resulting electrodes, which was estimated by using the Randles–Sevcik equation, also varied during the assembly process. Coating with PAMAM-Sil-rGO increased the electrochemical surface of GCE from 7.08 mm^2 to 8.93 mm^2, due to the high electroconductive properties of the graphene-based nanomaterial and the permeability of the grafted PAMAM moieties. Decoration of this material with Pt nanoparticles reduced the electrochemical surface area of the coated electrode to about 7.64 mm^2. This fact can be justified by the reduction of the permeability properties of the hybrid material due to filling of the interstitial space of the PAMAM moieties by the Pt nanoparticles. Immobilization of GOx on the electrode surface significantly reduced the electroactive surface area to about 4.81 mm^2, due to insulating characteristics of the protein molecules.

The barrier properties of the different electrode assemblies were also evaluated by EIS using the Randles equivalent circuit. Fig. 6 shows the corresponding Nyquist plots. All the experimental data were obtained by fitting with a conventional Randles equivalent circuit. As expected the charge transfer resistance measured at the bare GCE, R_{ct} = 84 Ω, was drastically reduced for the electrode

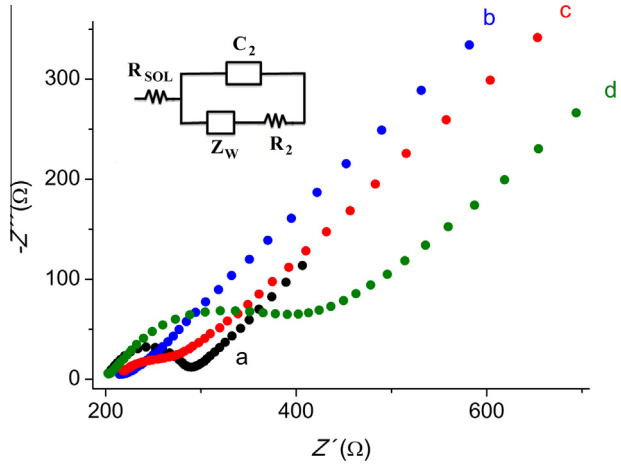

Fig. 6. Nyquist plots of bare GCE (a), PAMAM-Sil-rGO (b), PtNPs/PAMAM-Sil-rGO/GCE (c) and GOx/PtNPs/PAMAM-Sil-rGO/GCE (d) electrodes in 0.1 M KCl solution containing 5 mM $K_3[Fe(CN)_6]/K_4[Fe(CN)_6]$ (1:1).

coated with PAMAM-Sil-rGO, R_{ct} = 2 Ω, suggesting very low barrier properties for this hybrid nanomaterial. Moreover, a predominant straight line with slope near the unit was observed in a broad range of low frequencies. However, an increase in the barrier properties was noticed after decoration of the graphene-based hybrid nanomaterial with Pt nanoparticles, with R_{ct} = 90 Ω, which can be attributed to the above mentioned effect of the decrease in the permeability of the hybrid material upon intercalation of the Pt nanoparticles. Nevertheless, it should be highlighted that the electron transfer resistance of the PtNPs/PAMAM-Sil-rGO/GCE was similar to that of the bare electrode demonstrating high electroconductive properties of this inorganic–organic hybrid nanomaterial. Further immobilization of the enzyme caused a significant increase in the barrier properties of the electrode surface (R_{ct} = 244 Ω) due to coverage with the insulating protein molecules.

The optimal operational conditions for the GOx/PtNPs/PAMAM-Sil-rGO/GCE amperometric biosensor for glucose were also established. Fig. 7A shows the effect of the applied potential on the normalized amperometric response of the enzyme-modified electrode in buffered solution of pH 7.5 at room temperature. It should be pointed out that noisy and unstable signals were obtained by measuring the reduction of H_2O_2 with the prepared bioelectrode and, consequently, only the applied anodic potentials were tested. The anodic current increased when the applied potential increased from +200 mV to +400 mV vs. Ag/AgCl, reaching almost constant value at higher potentials. Then +400 mV was selected as optimum working potential. On the other hand, a higher amperometric response was observed for the electrode operated in buffered solutions of pH 7.5–8.0 (Fig. 7B), in agreement with the optimum value of pH reported for this enzyme. Accordingly, further experiments were performed at pH 7.5.

The analytical performance of enzyme biosensor constructed with the nanostructured electrode was evaluated under these optimal working conditions. Typical amperometric recordings to successive additions of glucose are shown in Fig. 8A. The electrode exhibited a fast electroanalytical response, reaching 95% of the steady-state current within 4 s. The resulting calibration curve, shown in Fig. 8B, exhibited a linear behavior (r = 0.998) in the broad range of glucose concentration between 10 μM and 8.1 mM glucose, according to the following equation:

$$I_A(\mu A) = 1.76 \cdot c(\text{Glucose/mM}) - 0.007.$$

A low detection limit of 0.8 μM glucose was estimated for this biosensor, according to the $3s_b/m$ criterion where s_b was estimated as the standard deviation for ten repetitive measurements of the lowest point in the calibration graph and m is the slope value of this calibration. The enzyme biosensor showed a sensitivity of 24.6 mA/M cm^2, which was calculated by using the electroactive surface area of the GOx/PtNPs/PAMAM-Sil-rGO/GCE. This high sensitivity can be attributed to the large electroactive surface area of the modified electrode, the synergic electrocatalytic effect of PtNPs and rGO for H_2O_2 oxidation, and the occurrence of fast electron transfer between the enzyme and the electrode surface due to the high electroconductive and low barrier properties of the 3D assembled hybrid nanomaterial.

The advantages of using this biosensor assembly were confirmed by immobilizing GOx at the different surfaces obtained during the construction of the analytical platform and further comparison of their electroanalytical responses toward successive addition of different volumes of 1 mM glucose solution. No significant amperometric response was observed for the bioelectrodes prepared without Pt nanoparticles, indicating that the nanoparticles played an essential role in the successful electrocatalytic decomposition of H_2O_2 on the electrode surface when poised at +400 mV.

To confirm this, the different electrode surfaces obtained during the assembly of the enzyme biosensor were also tested upon successive additions of 1 mM H_2O_2 solution. Fig. 9 shows the variation

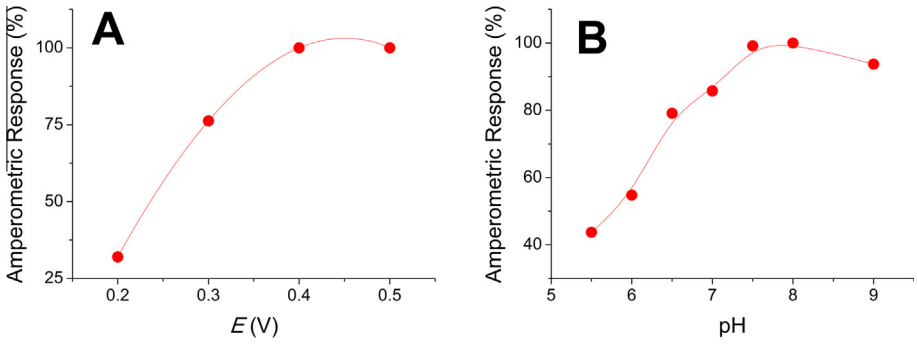

Fig. 7. Influence of the applied potential (A) at pH 7.5, and working pH (B) at E = +400 mV, on the amperometric response of the GOx/PtNPs/PAMAM-Sil-rGO/GCE enzyme electrode toward 1 mM glucose.

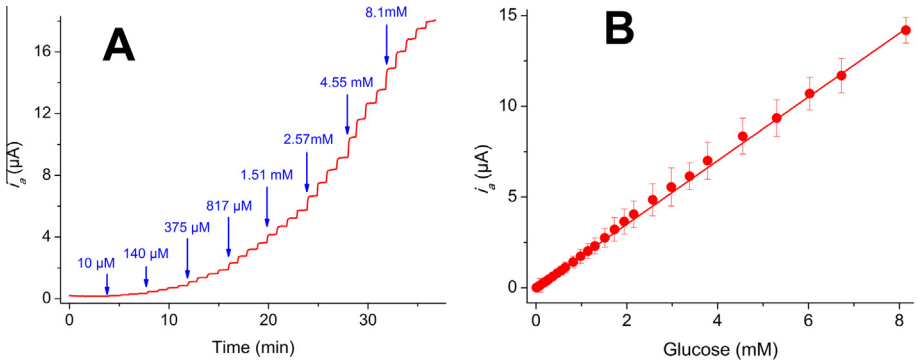

Fig. 8. A) Dynamic amperometric response of GOx/PtNPs/PAMAM-Sil-rGO/GCE poised at +400 mV to successive addition of different volumes of 1 mM glucose solution. B) Calibration curve constructed for glucose at the GOx/PtNPs/PAMAM-Sil-rGO/GCE biosensor.

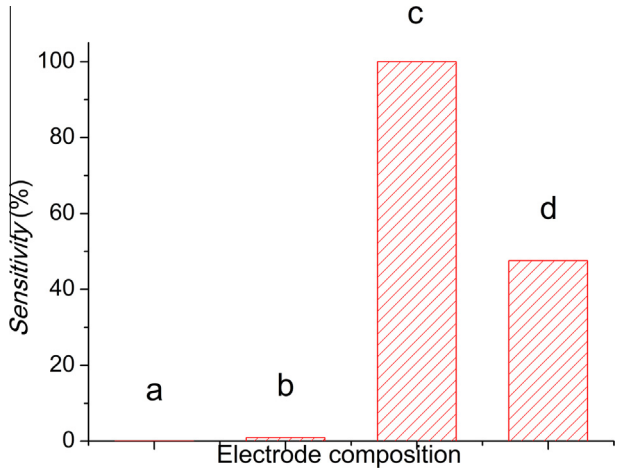

Fig. 9. Influence of the electrode composition on the slope value (normalized vs. the highest value) of the corresponding calibration graph obtained for H_2O_2. (a) GCE, (b) PAMAM-Sil-rGO/GCE, (c) PtNPs/PAMAM-Sil-rGO/GCE and (d) GOx/PtNPs/PAMAM-Sil-rGO/GCE.

in the slope values of the corresponding calibration plots obtained for H_2O_2. As it can be seen, the sensitivity achieved with the PtNPs/PAMAM-Sil-rGO/GCE electrode was almost twice than that with the GOx/PtNPs/PAMAM-Sil-rGO/GCE bioelectrode. Moreover, the sensitivity with the electrodes prepared without Pt nanoparticles (bar b) was less than 1% than that for the PtNPs/PAMAM-Sil-rGO/GCE electrode, thus confirming that Pt nanoparticles are involved in the electrocatalytic decomposition of H_2O_2 at the nanostructured surface poised at +400 mV. In addition, it becomes apparent that the immobilization of GOx reduced the capability of the hybrid nanomaterial to decompose H_2O_2, probably by masking the Pt nanoparticles located on the surface of the PAMAM dendrimer moieties.

The analytical performance of the GOx/PtNPs/PAMAM-Sil-rGO/GCE biosensor was compared with that of other published glucose sensors based on graphene-modified electrodes (Table 1). In general, it can be stated that the present biosensor shows similar or even better overall analytical behavior than other biosensors previously reported. Although the biosensors constructed by immobilizing GOx on polydopamine-graphene composite film [21] and palladium nanoparticle/chitosan-grafted graphene nanocomposites [22] showed an slightly better sensitivity, it should be pointed out that they operated at a much higher working potential of +700 mV, which has a detrimental effect on the selectivity of the biosensor device. The electrode prepared by immobilization of GOx in platinum nanoparticles/graphene/chitosan nanocomposite film showed a slightly better range of linear response but higher limit of detection that that achieved with the GOx/PtNPs/PAMAM-Sil-rGO/GCE biosensor working under similar operational conditions [12]. Moreover, it can be said that a potentiometric glucose sensor based on GOx immobilized on iron ferrite magnetic particle/chitosan composite modified gold coated GCE provided a large range of linearity [31].

On the other hand, an apparent Michaelis–Menten constant of K_M = 6.9 mM, and a maximum rate for the enzyme reaction of I_{MAX} = 16 µA were calculated for the GOx/PtNPs/PAMAM-Sil-rGO/GCE biosensor. This apparent K_M value was similar to those reported for the enzyme on a polydopamine–graphene composite film modified electrode (6.77 mM) [21] but lower than that reported for the enzyme immobilized on graphene quantum dots modified carbon ceramic electrode (0.76 mM) [29] and palladium nanoparticle/chitosan-grafted graphene nanocomposite modified GCE (1.2 mM) [22].

Table 1
Comparison of the analytical characteristics obtained for the GOx/PtNPs/PAMAM-Sil-rGO/GCE biosensor with those reported for other graphene-based enzyme electrodes for glucose determination.

Electrode	*E* (mV)	Linear range (mM)	Sensitivity (mA/Mcm^2)	LOD (μM)
Nafion/GOx/AuNPs/GF/GCE [23]	+800	0.001–30	–	1
GOx-Chi/pTBO/PB/rGO/GCE [24]	+200	0.02–1.09	59	8.4
GOx/TiO_2-GF/GCE [25]	−600	0–8	6.2	–
GOx-GF/Pt [26]	+400	0–22	8.045	–
GOx/Chi/GF/GCE [27]	−790	2–22	–	20
GOx/Chi-Fc/GO/GCE [28]	+300	0.02–6.78	10	7.6
GOx-GQD/CCE [29]	−420	0.005–1.27	85	1.73
GOx-pDA/GO/Au [21]	+700	0.001–4.7	28.4	0.1
GOx/Chi-AuNPs-GF/Au [11]	−200	2–10	–	180
GOx/PtNPs/Chi/GF/GCE [12]	+400	0.0006–5	–	0.6
GOx/PdNPs/Chi-GF/GCE [22]	+700	0.001–1	31.2	0.2
Nafion/GOx/APTES-GF/GCE [30]	−450	1–32	–	1
GOx/PtNPs/PAMAM-Sil-rGO/GCE	+400	0.01–8.1	24.6	0.8

GF: graphene; Chi: chitosan; pTBO: poly(toluidine blue O); PB: Prussian blue; Fc: ferrocene; GO: graphene oxide; GQD: graphene quantum dots; CCE: carbon ceramic electrode; pDA: polydopamine; APTES: 3-aminopropyltriethoxysilane.

The GOx/PtNPs/PAMAM-Sil-rGO/GCE biosensor exhibited a high reproducibility, with a relative standard deviation value of 5.8% (n = 10) for repetitive amperometric measurements of successive additions of 1 mM glucose. The assembly of the enzyme biosensor also showed acceptable reproducibility, with a relative standard deviation of 10.3% for ten different biosensors prepared in the same manner.

The selectivity of the biosensor was evaluated by measuring the amperometric current generated by different potential interfering substances in the presence of 500 μM glucose. The enzyme biosensor showed good selectivity, yielding unaffected amperometric response in the presence of fructose, sacarose, cafein and citric acid at 500 μM concentration. However, ascorbic acid and uric acid at a 1.0 μM concentration interfered in the quantification of glucose, giving rise to an increase of 6.4% and 17% in the measured current, respectively.

The long-term stability of the biosensor was estimated by storing the electrode at 4 °C under dry conditions. The electrode was periodically tested toward four consecutive additions 20 mM D-glucose solution. The biosensor retained more than 95% of the initial electroanalytical activity after one week of storage, but longer times at 4 °C produced a progressive loss of analytical response reaching about 52% of the initial activity after two weeks of storage.

The enzyme biosensor was employed to determine the total glucose content in a commercial soft drink (Pepsi), and the results were compared with those obtained with an enzymatic colorimetric assay kit. A total concentration of glucose of 189 ± 12 mM and 180 ± 3 mM was estimated with the electrochemical biosensor and the colorimetric kit, respectively. This result demonstrates the analytical reliability of the proposed electrochemical device to quantify glucose in real samples.

4. Conclusions

A novel inorganic–organic hybrid nanomaterial was prepared by decoration of PAMAM-modified graphene with platinum nanoparticles. This nanomaterial was employed to modify GCE, and further used as support for the glutaraldehyde-mediated immobilization of glucose oxidase. This enzyme electrode was employed to construct a mediator-free amperometric biosensor for glucose. The biosensor exhibited high sensitivity and reproducibility, a low detection limit, as well as fast electroanalytical response toward the analyte. These results suggest this novel hybrid nanomaterial can be employed to prepare sensitive and reliable oxidase-based enzyme biosensors.

Acknowledgements

R. Villalonga acknowledges to Ramón & Cajal contract from the Spanish Ministry of Science and Innovation. Financial support from the Spanish Ministry of Science and Innovation (CTQ2011-24355 and CTQ2012-34238), and Comunidad de Madrid S2009/PPQ-1642, Programme AVANSENS is gratefully acknowledged.

References

[1] K. Kerman, M. Saito, E. Tamiya, S. Yamamura, Y. Takamura, Trends Anal. Chem. 27 (2008) 585–592.
[2] J. Wang, Analyst 130 (2005) 421–426.
[3] A.K. Sarma, P. Vatsyayan, P. Goswami, S.D. Minteer, Biosens. Bioelectron. 24 (2009) 2313–2322.
[4] J. Wang, Small 1 (2005) 1036–1043.
[5] G. Liu, Y. Lin, Talanta 74 (2007) 308–317.
[6] M. Pumera, S. Sánchez, I. Ichinose, J. Tang, Sensor Actuat. B Chem. 123 (2007) 1195–1205.
[7] S. Campuzano, J. Wang, Electroanalysis 23 (2011) 1289–1300.
[8] A. Mehdi, C. Reye, R. Corriu, Chem. Soc. Rev. 40 (2011) 563–574.
[9] Y. Shao, J. Wang, H. Wu, J. Liu, I.A. Aksay, Y. Lin, Electroanalysis 22 (2010) 1027–1036.
[10] M. Pumera, A. Ambrosi, A. Bonanni, E.L.K. Chng, H.L. Poh, Trends Anal. Chem. 29 (2010) 954–965.
[11] C. Shan, H. Yang, D. Han, Q. Zhang, A. Ivaska, L. Niu, Biosens. Bioelectron. 25 (2010) 1070–1074.
[12] H. Wu, J. Wang, X. Kang, C. Wang, D. Wang, J. Liu, I.A. Aksay, Y. Lin, Talanta 80 (2009) 403–406.
[13] Z. Luo, L. Yuwen, Y. Han, J. Tian, X. Zhu, L. Weng, L. Wang, Biosens. Bioelectron. 36 (2012) 179–185.
[14] T. Liu, H. Su, X. Qu, P. Ju, L. Cui, S. Ai, Sensor Actuat. B Chem. 160 (2011) 1255–1261.
[15] S. Guo, Y. Du, X. Yang, S. Dong, E. Wang, Anal. Chem. 83 (2011) 8035–8040.
[16] E. Araque, R. Villalonga, M. Gamella, P. Martínez-Ruiz, J. Reviejo, J.M. Pingarrón, J. Mater. Chem. B 1 (2013) 2289–2296.
[17] W.S. Hummers, R.E. Offeman, J. Am. Chem. Soc. 80 (1958) 1339.
[18] B. Jiang, M. Wang, Y. Chen, J. Xie, Y. Xiang, Biosens. Bioelectron. 32 (2012) 305–308.
[19] R.M. Crooks, M. Zhao, L. Sun, V. Chechik, L.K. Yeung, Acc. Chem. Res. 34 (2001) 181–190.
[20] R.W. Scott, O.M. Wilson, R.M. Crooks, J. Phys. Chem. B. 109 (2005) 692–704.
[21] C. Ruan, W. Shi, H. Jiang, Y. Sun, X. Liu, X. Zhang, Z. Sun, L. Dai, D. Ge, Sensor Actuat. B Chem. 177 (2013) 826–832.
[22] Q. Zeng, J.S. Cheng, X.F. Liu, H.T. Bai, J.H. Jiang, Biosens. Bioelectron. 26 (2011) 3456–3463.
[23] T.T. Baby, S.S.J. Aravind, T. Arockiadoss, R.B. Rakhi, S. Ramaprabhu, Sensor Actuat. B Chem. 145 (2010) 71–77.
[24] X. Bai, G. Chen, K.K. Shiu, Electrochim. Acta 89 (2013) 454–460.
[25] H.D. Jang, S.K. Kim, H. Chang, K.M. Roh, J.W. Choi, J. Huang, Biosens. Bioelectron. 38 (2012) 184–188.
[26] Y. Liu, D. Yu, C. Zeng, Z. Miao, L. Dai, Langmuir 26 (2010) 6158–6160.
[27] S. Liu, J. Tian, L. Wang, Y. Luo, W. Lu, X. Sun, Biosens. Bioelectron. 26 (2011) 4491–4496.
[28] J.D. Qiu, J. Huang, R.P. Liang, Sensor Actuat. B Chem. 160 (2011) 287–294.
[29] H. Razmi, R. Mohammad-Rezaei, Biosens. Bioelectron. 41 (2013) 498–504.
[30] D. Zheng, S.K. Vashist, K. Al-Rubeaan, J.H.T. Luong, F.S. Sheu, Talanta 99 (2012) 22–28.
[31] K. Khun, Z.H. Ibupoto, J. Lu, M.S. AlSalhi, M. Atif, Anees A. Ansari, M. Willander, Sensor Actuat. B Chem. 173 (2012) 698–703.